

Tailored Local Bandgap Modulation as a Strategy to Maximize Luminescence Yields in Mixed-Halide Perovskites

Sascha Feldmann,* Timo Neumann, Richard Ciesielski, Richard H. Friend, Achim Hartschuh, and Felix Deschler*

Halide perovskites have emerged as high-performance semiconductors for efficient optoelectronic devices, not least because of their bandgap tunability using mixtures of different halide ions. Here, temperature-dependent photoluminescence microscopy with computational modelling is combined to quantify the impact of local bandgap variations from disordered halide distributions on the global photoluminescence yield in mixed-halide perovskite films. It is found that fabrication temperature, surface energy, and charge recombination constants are keys for describing local bandgap variations and charge carrier funneling processes that control the photoluminescence quantum efficiency. It is reported that further luminescence efficiency gains are possible through tailored bandgap modulation, even for materials that have already demonstrated high luminescence yields. The work provides a novel strategy and fabrication guidelines for further improvement of halide perovskite performance in light-emitting and photovoltaic applications.

as solar cells or light-emitting diodes, where high luminescence yields are a central figure of merit to quantify device performance of a material.^[1,2] Moreover, the bandgap of halide perovskites can be readily tuned throughout the entire visible spectrum by varying the ratio between different halide ions in the composition,^[3] making these materials particularly promising for lighting^[4] or optimized tandem solar cells with silicon.^[5]

In this work, we study the effects of local bandgap variations on photoluminescence yields in thin films of mixed-cation mixed-halide perovskites. Previous investigation with confocal photoluminescence (PL) microscopy and electron probe microanalysis reported the formation of micrometer-sized domains related to a varying halide ratio of bromide to iodide, which was

found to modulate the local optical bandgap.^[6] It was shown that this variation in bandgap induced by the halide demixing could be beneficial for maximizing photoluminescence quantum efficiency (PLQE) due to charge carrier funneling to low-bandgap regions. However, the driving factors for the formation of such energy landscape variations, and their influence on local carrier dynamics, remain largely unexplored. Yet, a clear picture how they impact device-relevant PLQEs is required to unlock the full potential of mixed-halide perovskites.

Using a combined experimental and modeling approach, we now quantify the influence of local bandgap variations together with the factors controlling it during fabrication, and show how exploiting this additional lever provides a novel and generalizable strategy to further maximize the performance of halide perovskites for optoelectronic applications.

1. Introduction

Halide perovskites have attracted attention as efficient semiconductors for optoelectronic applications in recent years, such

Dr. S. Feldmann, T. Neumann, Prof. R. H. Friend
Cavendish Laboratory
University of Cambridge
Cambridge CB30HE, UK
E-mail: sf561@cam.ac.uk

T. Neumann, Dr. F. Deschler
Walter Schottky Institute
Technical University of Munich
85748 Garching, Germany
E-mail: felix.deschler@wsi.tum.de

Dr. R. Ciesielski
Physikalisch-Technische Bundesanstalt (PTB)
10587 Berlin, Germany

Dr. R. Ciesielski, Prof. A. Hartschuh
Department of Chemistry and Center for NanoScience (CeNS)
LMU Munich
81377 Munich, Germany

 The ORCID identification number(s) for the author(s) of this article can be found under <https://doi.org/10.1002/adom.202100635>.

© 2021 The Authors. Advanced Optical Materials published by Wiley-VCH GmbH. This is an open access article under the terms of the Creative Commons Attribution License, which permits use, distribution and reproduction in any medium, provided the original work is properly cited.

DOI: 10.1002/adom.202100635

2. Results

We study films of the prototypical composition methylammonium-formamidinium lead bromide-iodide (nominally $\text{MA}_{0.17}\text{FA}_{0.83}\text{Pb}(\text{Br}_{0.17}\text{I}_{0.83})_3$, MAFA), prepared using a reported solution-processing protocol (see Supporting Information for details).^[7] First, we measure the local PL of a MAFA thin film (≈ 500 nm thick on glass substrate) using confocal microscopy (see Supporting Information for details) as a function of temperature (Figure 1).

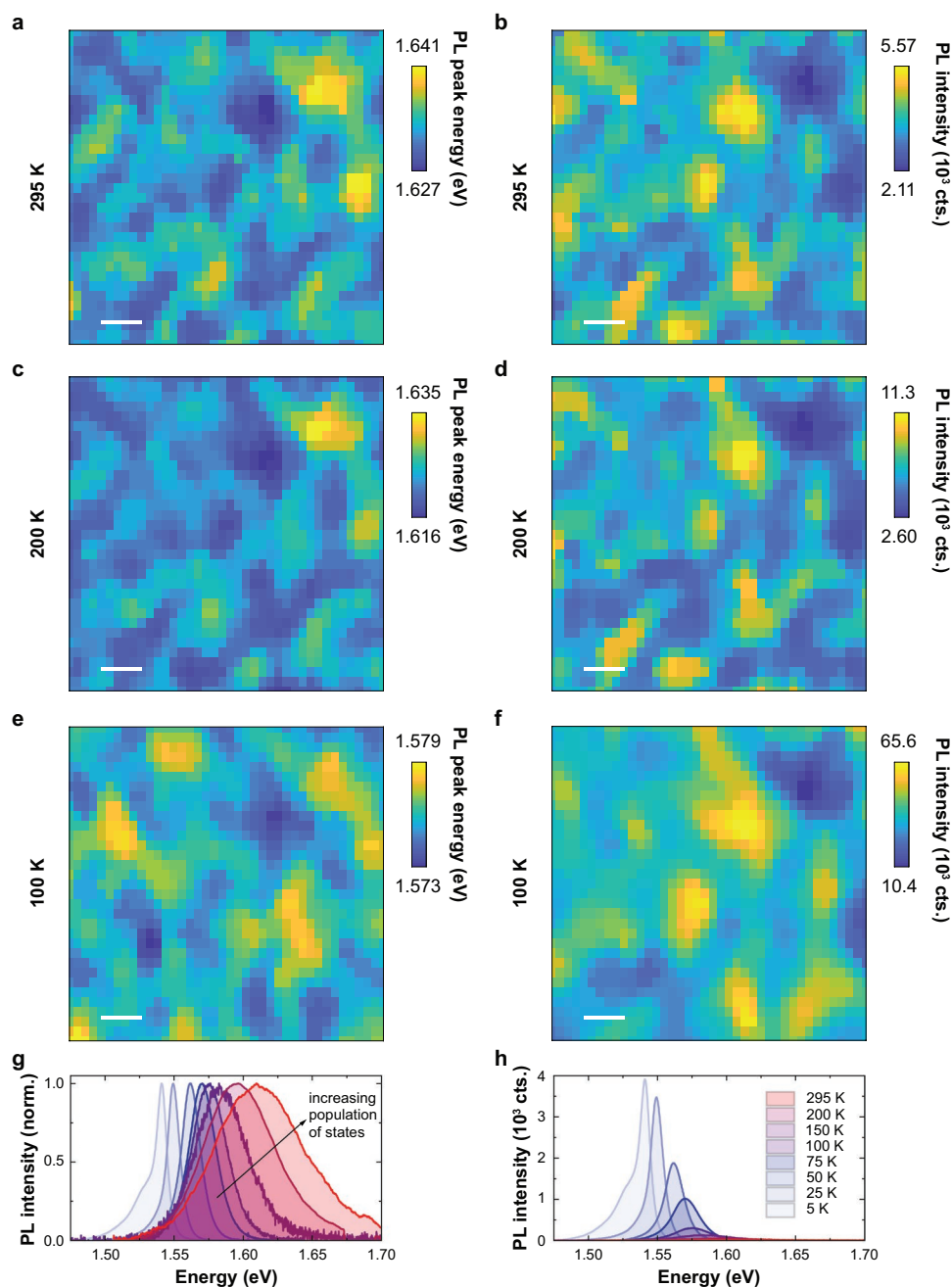


Figure 1. Carrier accumulation in low-bandgap regions. Temperature-dependent photoluminescence (PL) mapping of mixed-halide film confirms carrier accumulation in low-bandgap regions. a,c,e) PL peak energy maps, and b,d,f) PL intensity maps of $\text{MA}_{0.17}\text{FA}_{0.83}\text{Pb}(\text{Br}_{0.17}\text{I}_{0.83})_3$ film taken at three different temperatures, respectively, showing stronger emission from low-bandgap regions. g,h) Temperature-dependent evolution of normalized and absolute PL spectra averaged over the film, respectively. Samples were excited at 635 nm (250 kHz) with a carrier density of 10^{15} cm^{-3} . Scale bars are 2 μm .

We chose to study this specific composition because of the improved phase stability arising from the addition of the FA ion to the MA-based mixed-halide composition.^[8–11] This enables us to compare the PL spectra quantitatively at different temperatures. In addition, incorporation of the FA ion reduces the trap-density and thus increases the PLQE of the film, a prerequisite for observing the beneficial charge funneling.^[6,12–14]

We find that the PL spectrum gradually shifts its center of mass, i.e., the average position of all wavelengths of the

spectrum weighted according to their respective intensity values, to lower energies with decreasing temperature from 295 to 100 K (Figure 1a,c,e,g). These spectral changes can be explained with a temperature-activated process where charge carriers, with increasing thermal energy, can increasingly populate levels at higher energies in the distribution of states, that were previously inaccessible. Such partial asymmetric spectral changes are in contrast to the observations expected for a full spectral anti-Varshni-like bandgap shift with temperature, a

trend explained in the literature by reverse ordering of the band edges together with strong spin-orbit and electron–phonon coupling in perovskite-based semiconductors.^[15–17] Moreover, the spectral signatures we assign to the state-filling process are also unrelated to a phase-transition or emergence of an additional phase, which we start to observe only well below 100 K (Figure 1g). There, the entire spectrum starts to shift towards lower energies, culminating in the emergence of an additional higher-energy peak at 5 K, assigned previously to the presence of molecularly disordered orthorhombic domains.^[18]

The temperature-activated population of high-bandgap domains is further confirmed by the observed evolution of PL intensity, both locally and globally (Figure 1b,d,f,h). The overall PL enhancement with decreasing temperature can be explained by reduced nonradiative losses via phonon-mediated processes,^[16] typical for a direct-gap semiconductor. Importantly, we observe brighter emission from regions of lower bandgap with decreasing temperature, indicative of charge funneling to such sites of local energy minima. With decreasing temperature, this local PL intensity contrast becomes more pronounced, changing from an intensity ratio (max./min.) of 2.6 at 295 K, to 6.3 at 100 K. This finding is in line with reduced diffusion counteracting the charge funneling, as well as with a reduced carrier population spread of available energy states with decreasing kinetic energy, shown in the spectral mapping results.

Next, we aim to model the formation of the measured disordered energy landscape measured by following a phase-field approach^[19–23] based on the Langevin equation

$$\frac{d\phi}{dt} = -M(-\nabla^2)^a \frac{\delta F}{\delta \phi} + \eta \quad (1)$$

Here, the halide-dependent phase separation is modeled in terms of continuum fields instead of the true microscopic degrees of freedom. Within this approach, ϕ describes a slow variable, evolving over time (t). The driving force of the system is to minimize the total free energy F , which drives the rate of changes of slow variations. The mobility M is a function of all thermodynamic variables, including temperature and concentration. A random noise term η is added, which accounts for the microscopic fluctuations, i.e., fast variables like the temperature-dependent phonon modes. For $a = 1$, ϕ is a conserved field, for example here to describe the phase separation in binary alloys. Then, Equation (1) becomes the Cahn–Hilliard–Cook Equation,^[24,25] and ϕ represents the concentration of bromide or iodide ions. Notably, the rate of change of concentration is proportional to the divergence of a flux, which is the gradient of the chemical potential difference ($\Delta\mu$), itself a function of F . Within this model, we are able to model the demixing patterns and formation mechanism of the experimentally observed halide distributions in our samples, and can reproduce the measured energy landscapes (Figure 2).

The shift of the optical bandgap can be expected to be proportional to the ratio of iodide to bromide ions in the local composition.^[26] Hence, we can track the local bandgap following the evolution of chemical composition (Figure 2a,c,e) over time, and build up histograms of the occurrence of bandgap values (Figure 2b,d,f). Importantly, from the model we can derive two

major parameters that control the formed pattern and domain sizes, which in turn directly impact the optoelectronic performance of the film, as we report further below. The first factor is the temperature (T) which is part of the simulation via

$$\eta(\vec{r}_1, t_1) \eta(\vec{r}_2, t_2) = 2k_B T M \nabla^{2a} \delta(\vec{r}_1 - \vec{r}_2) \delta(t_1 - t_2) \quad (2)$$

with

$$\eta(\vec{r}, t) = 0 \quad (3)$$

where $\vec{r}_{1,2}$ describe the random positions at time steps $t_{1,2}$. A higher temperature during pattern formation thus leads to a faster domain formation, and, conversely, temperature quenching during film formation can be used to stop domain size growth by kinetic trapping. Multiple studies investigated the role of temperature on halide segregation in the past,^[8,27–29] although most of these relied on constant visible-light illumination as an external stimulus to drive this additional photo-induced segregation, while we focus here on halide patterns formed during film fabrication, and remain with a bromide fraction of ≈ 0.2 in the regime of a near-photostable composition at our employed excitation densities (see Figures S3 and S4 in the Supporting Information). Nonetheless, these studies observed an increasing extent of halide segregation at higher temperatures, which is captured by our phase-field model and which can be explained by increasing halide motion (likely mediated through vacancies) facilitating their demixing toward the respective thermodynamic energy minimum. At very high temperatures the entropy term, favoring remixing of halides, could in principle begin to dominate, but we are not aware of any study which investigated this exotic regime experimentally thus far.

The second key factor controlling the bandgap variations is based on the free energy

$$F(\phi) = \int d\vec{r} [f(\phi) + h(\nabla\phi, \nabla^2\phi, \dots)] \quad (4)$$

that is composed of a bulk (f) and surface (h) term, which we find to be sufficiently captured by

$$f = \frac{1}{2} \bar{r} \phi^2 + \frac{1}{4} \omega \phi^4 \quad (5)$$

$$h = \frac{1}{2} \kappa |\nabla\phi|^2 \quad (6)$$

with the phenomenological constants ρ , ω , and κ . This leads to the overall expression

$$\frac{d\phi}{dt} = -M(\rho\phi + \omega\phi^3 - \kappa\nabla^2\phi) + \eta \quad (7)$$

Thus, a second approach for controlling the domain sizes is via surface tension modulation. This could be achieved

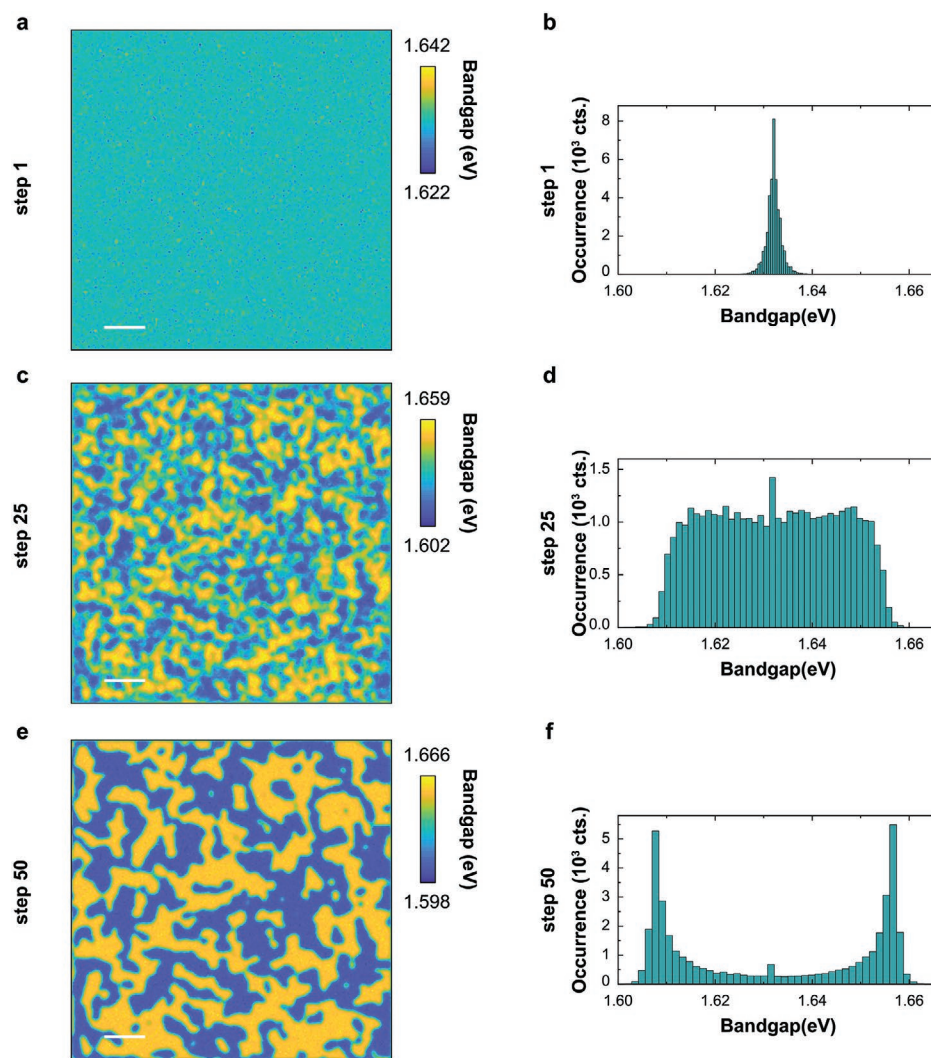


Figure 2. Simulation of local halide-ratio and bandgap variations in mixed-halide perovskites. a,c,e) Bandgap maps and b,d,f) corresponding histograms, using phase-field model based on a 2D-double-well free energy curve with composition fluctuations arising from thermal noise which evolves the microstructure into domains of varying halide composition with increasing temporal evolution steps. Scale bars are 2 μm .

through the use of surfactants, for example *n*-trioctylphosphine oxide (TOPO), used widely so far as Lewis base for trap-passivation in high-performance perovskite films.^[30,31] We propose that such reagents can also be used for controlling the extent of halide demixing to modulate the local bandgap instead, to achieve additional efficiency gains, and a recent study indeed hints at the effect of TOPO on halide segregation in these materials.^[32] Similarly, nucleation agents^[33,34] could also be added to control domain formation through tuning of the balance between the surface and bulk free energy terms, following the above equations. A recent study also showed that depositing a mixed-halide film on a nonwetting surface like poly[bis(4-phenyl)(2,4,6-trimethylphenyl)amine] reduces the extent of halide segregation, which becomes more pronounced again as the perovskite layer was increased.^[35] This observation could be connected to a surface tension modulation with respect to the perovskite/substrate interface, in line with our model predictions.

To gain quantitative insights on the impact of such heterogeneous energy landscapes on carrier recombination, we apply a drift-diffusion-recombination model based on the Continuity Equation to analyze the measured PL maps (Figure 3).

Based on a finite element approach, we model^[36] the recombination of free charge carriers in the varying energy landscape as

$$\frac{dn(\vec{r})}{dt} = G(\vec{r}, t, n, p) - R(\vec{r}, t, n, p) + D_n \frac{d^2 n(\vec{r}, t)}{d\vec{r}^2} + E\mu_n \frac{dn(\vec{r}, t)}{d\vec{r}} \quad (8)$$

with

$$D_{n,p} = \frac{\mu_{n,p} k_B T}{q} \quad (9)$$

Here, n and p , represent the concentration of electrons and holes at position \vec{r} , respectively, G describes the generation of

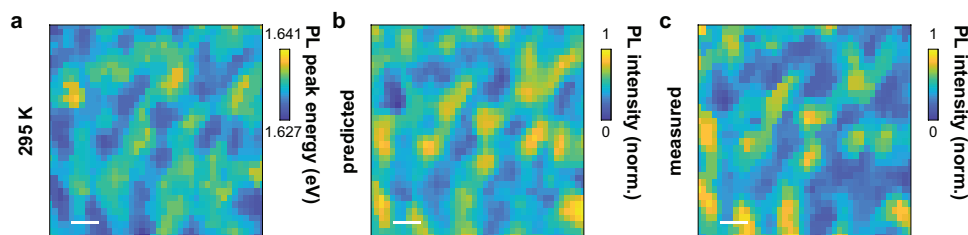


Figure 3. Quantification of photoluminescence (PL) modulation through bandgap heterogeneities. a) Measured energy landscape of MA_{0.17}FA_{0.83}Pb(Br_{0.17}I_{0.83})₃ at 295 K. b) Simulated PL intensity map using the drift-diffusion model and PL energy map presented in a). c) Measured PL intensity map of the sample area showing good agreement with the model predictions in b). Scale bars are 2 μm .

charge carrier pairs upon optical excitation, and R denotes the recombination of charges. D is the material-specific diffusion constant, connected to the mobility $\mu_{n,p}$ of electrons or holes, respectively, via the Boltzmann constant k_B and charge q . E represents the strength of the electric field at each position, and is thus directly correlated with the energy potential variation, which we map out (Figure 3a). The recombination rate is itself a sum of radiative and nonradiative recombination events via

$$R = k_1(n + p) + k_2(n \times p) \quad (10)$$

where k_1 and k_2 are nonradiative and radiative recombination rates, respectively. We omitted a third-order Auger term, as its contribution is negligible at our low excitation density of 10^{15} cm^{-3} (see Supporting Information for details on the modeling and literature values used for constants). We note that even upon significant funneling-induced concentration of carriers in low-bandgap regions, discussed in detail below, Auger recombination remains insignificant. Moreover, it was found experimentally that predominantly holes accumulate in the low-bandgap regions, while electrons remain mostly mobile.^[6] Thus, the observed energy variation arising from the halide demixing must be predominantly modulating the valence band offset, leaving the conduction band level mostly unchanged across the film, and we account for this in our model. This can also be rationalized by the dominant contribution of halide atomic orbitals to the formation of the valence band maximum.^[37]

Based on the experimentally determined energy landscape, we find excellent agreement between the simulated and observed PL intensity distributions (Figure 3b,c), indicating that our model is a robust description of the locally modulated carrier dynamics. With this, we can now run entirely in silico experiments by producing an energy landscape using the phase-field model introduced above under changing fabrication conditions, and use the drift-diffusion-recombination model to predict the corresponding PL performance of that film (see Figure S2, Supporting Information). Our simulation presents a powerful tool for discovering optimized film preparation conditions, with impact for a wide range of current and future halide perovskite materials.

We now apply the combined pattern formation and recombination model on our investigated mixed-halide perovskites films to gain quantitative insights into the impact of local bandgap variations on the global PLQE, one of the most important performance indicators for optoelectronic applications (Figure 4).

The PLQE is defined as the ratio of radiative to the sum of radiative and nonradiative decay channels

$$\text{PLQE} = \frac{k_2(n \times p)}{k_1(n + p) + k_2(n \times p)} \quad (11)$$

We note that, with the term “PLQE” we refer to the internal PLQE throughout this study. The external PLQE is related to this quantity by considering light-outcoupling and photon recycling events,^[38–40] which will impact the absolute measured values but not the trends and mechanisms described here. Based on the experimentally mapped energy landscape, we calculate the relative changes to the global PLQE of the film when varying the degree of energy variation (ΔE_g , determined as the standard deviation of the bandgap distribution), compared to a hypothetical, flat energy landscape (Figure 4a). Notably, we find the PLQE to increase significantly as a function of the funneling potential. We find that the measured ΔE_g of $\approx 3 \text{ meV}$ —which forms spontaneously for our used mixed-halide MAFA fabrication protocol—is already benefitting the observed PLQE, increasing it by about 2% in relative terms. For further increases in the charge funneling potential, additional PLQE gains are achievable, for example by up to 10% when increasing the energy variation by as little as 10 meV, possible by tuning the local halide ratio during fabrication.

The magnitude of these improvements further depends on the interplay between electron and hole trap densities in the film, which are a direct consequence of the material fabrication conditions (Figure 4c,d). Hence, our model is not relying on a common recombination constant k_1 , as presented in the simplified Equation (10) above, but instead distinguishes between the respective electron and hole lifetimes (see Supporting Information for details). In line with the earlier report that mostly the valence band off-sets are modulated by the bandgap variation,^[6] longer hole lifetimes (τ_h) than electron lifetimes (τ_e) are found to be favorable and result in the largest PLQE improvements with charge funneling potential. This delicate interplay between electron and hole lifetimes also implies that a much shorter hole than electron lifetime—corresponding to a higher density of or energetically deeper lying hole traps—will instead reduce the global PLQE, compared to a scenario with flat energy landscape and hence no charge funneling. Thus we observe negative relative PLQE values in these regimes (Figure 4a,c,d). Notably, this finding also coincides with previously reported carrier lifetimes of halide perovskites in the literature, where $\tau_h > \tau_e$.^[41] We thus expect the beneficial charge funneling, which we quantify

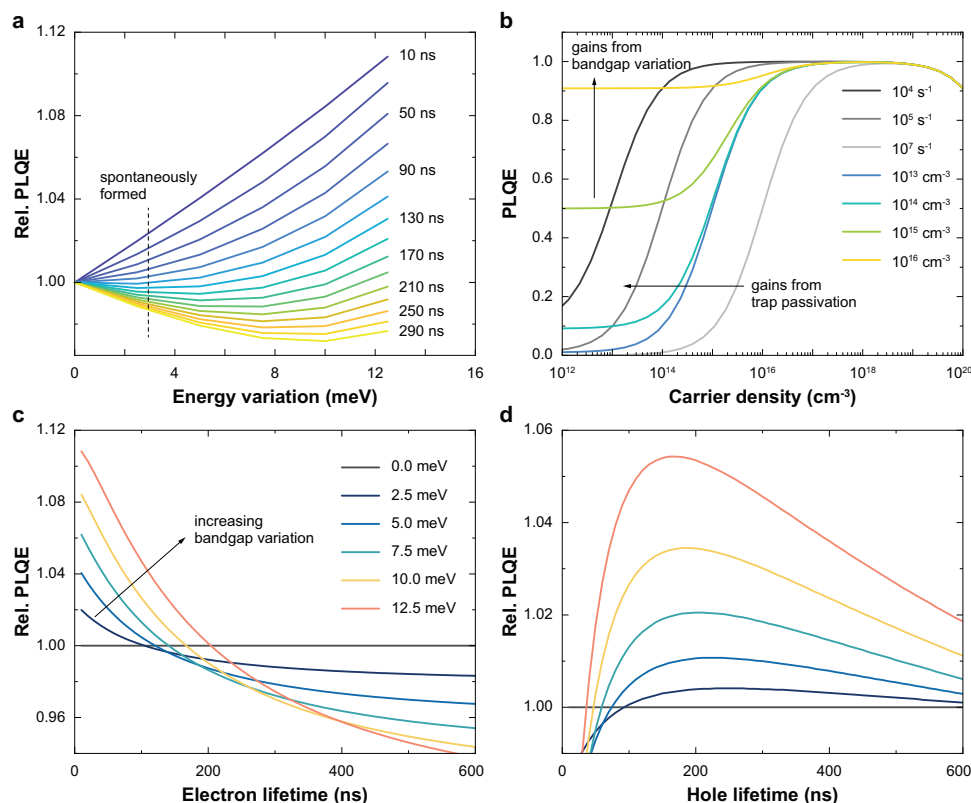


Figure 4. Maximizing global PLQE through energy-landscape modulation. a) Relative photoluminescence quantum efficiency (PLQE) dependence on energy variation (ΔE_g), compared to the film without bandgap variation for different electron lifetimes (τ_e). Hole lifetime (τ_h) set to 100 ns. Dashed line indicates experimentally found value of ΔE_g . b) Comparison between established trap-passivation approaches (reducing k_1 , gray scale) and novel bandgap variation (increasing doping density, colored) for improving PLQE. Based on Equation (10), with inclusion of a doping term^[6] to account for the local charge accumulation. c,d) Relative PLQE as function of electron and hole lifetime, respectively, for different degrees of bandgap variation. Results are based on experimental $\text{MA}_{0.17}\text{FA}_{0.83}\text{Pb}(\text{Br}_{0.17}\text{I}_{0.83})_3$ photoluminescence mapping at 295 K.

here, to have already contributed to the very high PLQE values reported for mixed-halide perovskites since their discovery.

Our results should be clearly distinguished from the trap-passivation strategies mostly explored so far to increase PLQEs (trends sketched in Figure 4b). Those established approaches focus on reducing the nonradiative rate constant k_1 of the material, for example by filling atomic vacancies in the film which act as electron or hole traps.^[42,43] This will improve the PLQE, as shown, by shifting its maximum value to lower carrier densities. The bandgap modulation approach we discuss here now provides an additional pathway to maximizing PLQEs by shifting them vertically with increasing accumulation of charges. Thus, it provides a strategy to further increase the optoelectronic performance of mixed-halide films that have already been optimized for low trap densities (i.e., mixed-cationic compositions), since our approach affects also the radiative recombination rates, making the materials brighter overall.

3. Conclusions

In summary, we report the impact of charge funneling from local energy variations in mixed-halide perovskite films on their global PL yields. By combining local PL mapping with

phase-field and drift-diffusion-recombination modeling, we can fully describe the observed PL intensity patterns based on bandgap variations as a consequence of halide demixing. From our model, we identify temperature, surface energy, and recombination constants as key factors to control the formed energy variations and can predict their influence on the PLQE. We conclude that significant PLQE enhancements are achievable through tailored bandgap modulation as a novel strategy to further increase the performance of these materials for highly efficient optoelectronics applications.

Supporting Information

Supporting Information is available from the Wiley Online Library or from the author.

Acknowledgements

S.F. acknowledges funding from the Studienstiftung des deutschen Volkes, as well as support from the Winton Programme for the Physics of Sustainability. S.F. and R.H.F. are grateful for funding from the Engineering and Physical Sciences Research Council (EPSRC UK, Grant ref. EP/R044481/1) and S.F. moreover acknowledges funding via an

EPSRC Doctoral Prize Fellowship. R.C. and A.H. gratefully acknowledge financial support from the Deutsche Forschungsgemeinschaft (DFG) via e-conversion-EXC No. 2089/1-390776260 and from the Bavarian research network SolTech. F.D. acknowledges funding from the Winton Programme for the Physics of Sustainability and the DFG Emmy Noether Program.

Open access funding enabled and organized by Projekt DEAL.

Conflict of Interest

The authors declare no conflict of interest.

Authors Contribution

S.F. and F.D. conceived and planned the experiments with additional input from R.H.F. and A.H. S.F. fabricated samples. S.F. and R.C. performed confocal microscopy measurements. S.F., T.N., and R.C. analyzed the data. S.F. developed the phase-field and T.N. the drift-diffusion model. S.F. wrote the manuscript and compiled figures, with discussion of results and feedback on the manuscript from all authors.

Data Availability Statement

The data that support the findings of this study are available from the authors upon reasonable request.

Keywords

halide perovskites, halide segregation, optoelectronics, photoluminescence

Received: March 29, 2021

Revised: April 30, 2021

Published online:

- [1] S. D. Stranks, H. J. Snaith, *Nat. Nanotechnol.* **2015**, *10*, 391.
- [2] L. N. Quan, B. P. Rand, R. H. Friend, S. G. Mhaisalkar, T.-W. Lee, E. H. Sargent, *Chem. Rev.* **2019**, *119*, 7444.
- [3] N. Kitazawa, Y. Watanabe, Y. Nakamura, *J. Mater. Sci.* **2002**, *37*, 3585.
- [4] Z.-K. Tan, R. S. Moghaddam, M. L. Lai, P. Docampo, R. Higler, F. Deschler, M. Price, A. Sadhanala, L. M. Pazos, D. Credgington, F. Hanusch, T. Bein, H. J. Snaith, R. H. Friend, *Nat. Nanotechnol.* **2014**, *9*, 687.
- [5] A. Al-Ashouri, E. Köhnen, B. Li, A. Magomedov, H. Hempel, P. Caprioglio, J. A. Márquez, A. B. M. Vilches, E. Kasparavicius, J. A. Smith, N. Phung, D. Menzel, M. Grischek, L. Kegelman, D. Skroblin, C. Gollwitzer, T. Malinauskas, M. Jošt, G. Matič, B. Rech, R. Schlattmann, M. Topič, L. Korte, A. Abate, B. Stannowski, D. Neher, M. Stollerfoht, T. Unold, V. Getautis, S. Albrecht, *Science* **2020**, *370*, 1300.
- [6] S. Feldmann, S. Macpherson, S. P. Senanayak, M. Abdi-Jalebi, J. P. H. Rivett, G. Nan, G. D. Tainter, T. A. S. Doherty, K. Frohna, E. Ringe, R. H. Friend, H. Sirringhaus, M. Saliba, D. Beljonne, S. D. Stranks, F. Deschler, *Nat. Photonics* **2020**, *14*, 123.
- [7] M. Saliba, T. Matsui, J.-Y. Seo, K. Domanski, J.-P. Correa-Baena, M. K. Nazeeruddin, S. M. Zakeeruddin, W. Tress, A. Abate, A. Hagfeldt, M. Grätzel, *Energy Environ. Sci.* **2016**, *9*, 1989.
- [8] E. T. Hoke, D. J. Slotcavage, E. R. Dohner, A. R. Bowring, H. I. Karunadasa, M. D. McGehee, *Chem. Sci.* **2015**, *6*, 613.
- [9] K. Galkowski, A. Mitioglu, A. Miyata, P. Plochocka, O. Portugall, G. E. Eperon, J. T.-W. Wang, T. Stergiopoulos, S. D. Stranks, H. J. Snaith, R. J. Nicholas, *Energy Environ. Sci.* **2016**, *9*, 962.
- [10] S. Tombe, G. Adam, H. Heilbrunner, D. H. Apaydin, C. Ulbricht, N. S. Sariciftci, C. J. Arendse, E. Iwuoha, M. C. Scharber, *J. Mater. Chem. C* **2017**, *5*, 1714.
- [11] A. J. Knight, J. Borchert, R. D. J. Oliver, J. B. Patel, P. G. Radaelli, H. J. Snaith, M. B. Johnston, L. M. Herz, *ACS Energy Lett.* **2021**, *6*, 799.
- [12] M. Salado, L. Calio, R. Berger, S. Kazim, S. Ahmad, *Phys. Chem. Chem. Phys.* **2016**, *18*, 27148.
- [13] N. Pellet, P. Gao, G. Gregori, T.-Y. Yang, M. K. Nazeeruddin, J. Maier, M. Grätzel, *Angew. Chem., Int. Ed.* **2014**, *53*, 3151.
- [14] T. J. Jacobsson, S. Svanström, V. Andrei, J. P. H. Rivett, N. Kornienko, B. Philippe, U. B. Cappel, H. Rensmo, F. Deschler, G. Boschloo, *J. Phys. Chem. C* **2018**, *122*, 13548.
- [15] J. Even, L. Pedesseau, M.-A. Dupertuis, J.-M. Jancu, C. Katan, *Phys. Rev. B* **2012**, *86*, 205301.
- [16] R. L. Milot, G. E. Eperon, H. J. Snaith, M. B. Johnston, L. M. Herz, *Adv. Funct. Mater.* **2015**, *25*, 6218.
- [17] W. A. Saidi, S. Poncé, B. Monserrat, *J. Phys. Chem. Lett.* **2016**, *7*, 5247.
- [18] M. I. Dar, G. Jacopin, S. Meloni, A. Mattoni, N. Arora, A. Boziki, S. M. Zakeeruddin, U. Rothlisberger, M. Grätzel, *Sci. Adv.* **2016**, *2*, e1601156.
- [19] Y. Oono, S. Puri, *Phys. Rev. Lett.* **1987**, *58*, 836.
- [20] K. R. Elder, T. M. Rogers, R. C. Desai, *Phys. Rev. B* **1988**, *38*, 4725.
- [21] K. Elder, H. Gould, J. Tobochnik, *Comput. Phys.* **1993**, *7*, 27.
- [22] K. Narita, T. Koyama, Y. Tsukada, *Mater. Trans.* **2013**, *54*, 661.
- [23] G. Jiang, F. Yan, S. Wan, Y. Zhang, M. Yan, *Phys. Chem. Chem. Phys.* **2019**, *21*, 10902.
- [24] J. W. Cahn, J. E. Hilliard, *J. Chem. Phys.* **1958**, *28*, 258.
- [25] H. E. Cook, *Acta Metall.* **1970**, *18*, 297.
- [26] L. Vegard, *Z. Phys.* **1921**, *5*, 17.
- [27] T. Elmelund, B. Seger, M. Kuno, P. V. Kamat, *ACS Energy Lett.* **2020**, *5*, 56.
- [28] A. J. Barker, A. Sadhanala, F. Deschler, M. Gandini, S. P. Senanayak, P. M. Pearce, E. Mosconi, A. J. Pearson, Y. Wu, A. R. S. Kandada, T. Leijtens, F. De Angelis, S. E. Dutton, A. Petrozza, R. H. Friend, *ACS Energy Lett.* **2017**, *2*, 1416.
- [29] C. G. Bischak, C. L. Hetherington, H. Wu, S. Aloni, D. F. Ogletree, D. T. Limmer, N. S. Ginsberg, *Nano Lett.* **2017**, *17*, 1028.
- [30] D. W. deQuilettes, S. Koch, S. Burke, R. K. Paranjy, A. J. Shropshire, M. E. Ziffer, D. S. Ginger, *ACS Energy Lett.* **2016**, *1*, 438.
- [31] I. L. Braly, D. W. deQuilettes, L. M. Pazos-Outón, S. Burke, M. E. Ziffer, D. S. Ginger, H. W. Hillhouse, *Nat. Photonics* **2018**, *12*, 355.
- [32] R. A. Belisle, K. A. Bush, L. Bertoluzzi, A. Gold-Parker, M. F. Toney, M. D. McGehee, *ACS Energy Lett.* **2018**, *3*, 2694.
- [33] N. D. Treat, J. A. N. Malik, O. Reid, L. Yu, C. G. Shuttle, G. Rumbles, C. J. Hawker, M. L. Chabiny, P. Smith, N. Stingelin, *Nat. Mater.* **2013**, *12*, 628.
- [34] S. Masi, A. Rizzo, R. Munir, A. Listorti, A. Giuri, C. E. Corcione, N. D. Treat, G. Gigli, A. Amassian, N. Stingelin, S. Colella, *Adv. Energy Mater.* **2017**, *7*, 1602600.
- [35] M. Hu, C. Bi, Y. Yuan, Y. Bai, J. Huang, *Adv. Sci.* **2015**, *3*, 6.
- [36] T. Kirchartz, J. A. Márquez, M. Stollerfoht, T. Unold, *Adv. Energy Mater.* **2020**, *10*, 1904134.
- [37] R. E. Brandt, V. Stevanović, D. S. Ginley, T. Buonassisi, *MRS Commun.* **2015**, *5*, 265.
- [38] L. M. Pazos-Outón, M. Szumilo, R. Lamboll, J. M. Richter, M. Crespo-Quesada, M. Abdi-Jalebi, H. J. Beeson, M. Vrućinić, M. Alsari, H. J. Snaith, B. Ehrler, R. H. Friend, F. Deschler, *Science* **2016**, *351*, 1430.

- [39] J. M. Richter, M. Abdi-Jalebi, A. Sadhanala, M. Tabachnyk, J. P. H. Rivett, L. M. Pazos-Outón, K. C. Gödel, M. Price, F. Deschler, R. H. Friend, *Nat. Commun.* **2016**, 7, 13941.
- [40] C. L. Davies, M. R. Filip, J. B. Patel, T. W. Crothers, C. Verdi, A. D. Wright, R. L. Milot, F. Giustino, M. B. Johnston, L. M. Herz, *Nat. Commun.* **2018**, 9, 293.
- [41] F. Staub, H. Hempel, J.-C. Hebig, J. Mock, U. W. Paetzold, U. Rau, T. Unold, T. Kirchartz, *Phys. Rev. Appl.* **2016**, 6, 44017.
- [42] F. Gao, Y. Zhao, X. Zhang, J. You, *Adv. Energy Mater.* **2020**, 10, 1902650.
- [43] D. Luo, R. Su, W. Zhang, Q. Gong, R. Zhu, *Nat. Rev. Mater.* **2020**, 5, 44.